Ciliary beat pattern and frequency in genetic variants of primary ciliary dyskinesia

Johanna Raidt[1], Julia Wallmeier[1], Rim Hjeij[1], Jörg Große Onnebrink[1], Petra Pennekamp[1], Niki T. Loges[1], Heike Olbrich[1], Karsten Häffner[2], Gerard W. Dougherty[1], Heymut Omran[1] and Claudius Werner[1]

Affiliations: [1]University Children's Hospital Münster, Dept of General Pediatrics, Pediatric Pulmonology Unit, Münster, Germany. [2]Dept of Pediatrics, University Hospital Freiburg, Freiburg, Germany.

Correspondence: Claudius Werner, University Children's Hospital Münster, Dept of General Pediatrics, Albert-Schweitzer-Campus 1, Geb. A1, D-48149 Münster, Germany.
E-mail: claudius.werner@ukmuenster.de

ABSTRACT Primary ciliary dyskinesia (PCD) is a rare genetic disorder leading to recurrent respiratory tract infections. High-speed video-microscopy analysis (HVMA) of ciliary beating, currently the first-line diagnostic tool for PCD in most centres, is challenging because recent studies have expanded the spectrum of HVMA findings in PCD from grossly abnormal to very subtle. The objective of this study was to describe the diversity of HVMA findings in genetically confirmed PCD individuals.

HVMA was performed as part of the routine work-up of individuals with suspected PCD. Subsequent molecular analysis identified biallelic mutations in the PCD-related genes of 66 individuals. 1072 videos of these subjects were assessed for correlation with the genotype.

Biallelic mutations (19 novel) were found in 17 genes: *DNAI1*, *DNAI2*, *DNAH5*, *DNAH11*, *CCDC103*, *ARMC4*, *KTU/DNAAF2*, *LRRC50/DNAAF1*, *LRRC6*, *DYX1C1*, *ZMYND10*, *CCDC39*, *CCDC40*, *CCDC164*, *HYDIN*, *RSPH4A* and *RSPH1*. Ciliary beat pattern variations correlated well with the genetic findings, allowing the classification of typical HVMA findings for different genetic groups. In contrast, analysis of ciliary beat frequency did not result in additional diagnostic impact.

In conclusion, this study provides detailed knowledge about the diversity of HVMA findings in PCD and may therefore be seen as a guide to the improvement of PCD diagnostics.

@ERSpublications
PCD is associated with a variety of ciliary beat pattern abnormalities which correlate with genetic subtypes http://ow.ly/zh5jP

For editorial comments see page 1418.

This article has supplementary material available from erj.ersjournals.com

Received: Jan 16 2014 | Accepted after revision: July 02 2014 | First published online: Sept 03 2014

Support statement: This work was supported by European Commission FP7 (Seventh Framework Programme for Research) grant no. 305404 (BESTCILIA) to Heymut Omran, European Commission FP7 grant no. 241955 (SYSCILIA) to Heymut Omran, the "Deutsche Forschungsgemeinschaft" (DFG OM 6/4, OM 6/5) and the IZKF Münster (Om2/009/12).

Conflict of interest: None declared.

Introduction

Primary ciliary dyskinesia (PCD) (MIM 244400) is a rare genetic disorder of ciliary motility resulting in neonatal respiratory distress, chronic upper and lower respiratory tract disease, male infertility, and organ laterality defects in almost 50% of cases (Kartagener's Syndrome) [1].

PCD is both under-diagnosed and diagnosed too late [2]. Direct visualisation of ciliary beat pattern (CBP) and frequency (CBF) by high-speed video-microscopy analysis (HVMA) has been recommended as a first-line diagnostic test, along with transmission electron microscopy (TEM) [3]. Further methods that complete the armamentarium for PCD diagnosis include immunofluorescence (IF) microscopy, genetics and measurement of nasal nitric oxide (nNO) production [4].

Although HVMA is increasingly applied, it is a challenging method for various reasons: 1) chronic infection and inflammation often result in additional secondary ciliary damage, which obscures the primary beat abnormality [1, 5]; 2) standardised procedures between centres are lacking; 3) there is a shortage of quantitative data for the interpretation of CBPs; and 4) HVMA abnormalities may be subtle in recently identified variants.

Mutations in multiple genes have been described as being a cause of autosomal recessive, nonsyndromic PCD. Mutations in nine genes affect outer dynein arm (ODA) components: *DNAI1*, *DNAI2*, *DNAH5*, *DNAL1*, *CCDC103*, *NME8/TXNDC3*, *CCDC114* and *ARMC4* [1, 6, 7] result in ODA defects, whereas *DNAH11* mutations result in PCD with normal ultrastructure [8]. Nine genes encode the cytoplasmic proteins required for the assembly of both ODA and inner dynein arm (IDA) complexes: *KTU/DNAAF1*, *LRRC50/DNAAF2*, *C19orf51/DNAAF3*, *LRRC6*, *HEATR2*, *DYX1C1/DNAAF4*, *ZMYND10*, *SPAG1* and *C21orf59* [1, 9–12]. Mutations in *CCDC39* and *CCDC40* result in an IDA and microtubular disorganisation defect [13, 14]. Mutations in *CCDC164* and *CCDC65* result in nexin link defects [15, 16]. Mutations in *HYDIN* cause a deficiency of the C2b projection of the central pair (CP) microtubules [17]. *RSPH9, RSPH4A* [18] and *RSPH1* [19] affect radial spoke protein components. Mutations in genes affecting flagellar motility, such as *DNAH1* (IDA component) [20], have not yet been linked to PCD.

In this study, we correlated the findings of the HVMA with a diverse set of genetic PCD variants using Sisson-Ammons Video Analysis (SAVA) (Ammons Engineering, Mt Morris, MI, USA) [21], a widely-accepted system for ciliary beat analysis. These videos were acquired during clinical routine PCD work-up. It was not the aim of the study to systematically re-evaluate SAVA or to compare it to other systems.

Methods

Subjects

Subjects were referred to our centre for PCD work-up. PCD diagnosis was based on typical clinical features and PCD-specific abnormal findings in at least two of the following methods: nNO measurement, HVMA, TEM or IF microscopy. Videos from 10 individuals without acute or chronic respiratory symptoms (healthy controls (HCs)) and 10 individuals with respiratory symptoms but in whom PCD was excluded (disease controls (DCs)) were included for comparison. Although DCs were referred for PCD work-up, none displayed key PCD characteristics (situs abnormality, neonatal respiratory distress, both upper and lower airways problems). Beyond that, PCD was ruled out by at least one additional finding: high nNO values, normal TEM or IF. As ultrastructural analysis using TEM or IF microscopy may be unremarkable in PCD [1, 8, 15–17] or even misleading [22], we only analysed individuals with confirmed biallelic mutations. The study was approved by the Ethics Committee of the Westphalian Wilhelms University of Münster (Münster, Germany). Written informed consent to participate in this study was obtained from each individual or by the legal guardian of subjects under 18 years or age.

Nasal brush biopsy and high-speed video-microscopy analysis

Ciliated respiratory epithelial cells were obtained by nasal brush biopsy using a cytology brush, and were suspended in RPMI 1640 medium. HVMA was carried out directly after brushing. Videos were recorded using a Basler scA640-120 fm digital high-speed video camera (Basler AG, Ahrensburg, Germany) attached to an inverted phase-contrast microscope (Zeiss Axio Vert. A1; Carl Zeiss AG, Göttingen, Germany) equipped with a 40× objective. Digital image sampling was performed at 120–150 frames per second (fps) and a 640 × 480 pixel resolution. Image processing was performed using SAVA [21]. The temperature was maintained at 25°C by a Pecon Temp Controller 2000-2 (PeCon GmbH, Erbach, Germany). The ciliary beat was evaluated by views from both the side and the top in real time and in slow motion playback. CBP was described using the following terms: recognisability of regular forward and recovery strokes; static cilia; almost static cilia with minimal movements; stiff beating due to a reduced bending capacity/amplitude; abnormal circular beating. The quality of the video samples was scored using an adapted classification system [5]: excellent (ciliated cell bundle without projections), good (ciliated cell bundle with minor

DOI: 10.1183/09031936.00052014

projections), acceptable (ciliated cell bundle with major projections), insufficient (isolated ciliated cell within an epithelial strip or single cell). Insufficient videos were excluded from the analysis. HVMA was performed independently by two investigators: J. Raidt or J. Wallmeier, and C. Werner or H. Omran. In all cases, HVMA was performed prior to genetic testing. Results from the HVMA were not modified by knowledge of the genetic result. Samples were only taken in individuals who were not receiving nasal steroids or decongestants, and who did not show signs of acute respiratory infection for at least 3 weeks in order to minimise secondary ciliary dyskinesia.

Mutational analysis

Mutational analysis was performed after whole genome linkage analysis as described elsewhere [6] or by using a direct candidate gene approach. DNA was isolated from blood samples or from lymphocyte cultures standard methods. Amplification of coding exons, including the exon–intron boundaries, was performed using a volume of 50 μL containing 30 ng of DNA, 50 pmol of each primer, 2 mM dNTPs and 1.0 U GoTaq DNA polymerase (Promega Corporation, Madison, WI, USA). PCR conditions and primer details are available upon request. PCR products were verified by agarose gel electrophoresis, purified using ExoSAP-IT (Affymetrix, Santa Clara, CA, USA) and sequenced bidirectionally using the BigDye Terminator v3.1 Cycle Sequencing kit (Applied Biosystems, Life Technologies Ltd, Paisley, UK). Samples were separated and analysed on an Applied Biosystems 3730xl DNA Analyser. Sequence data were evaluated using CodonCode software (www.codoncode.com). Only biallelic mutations that could be clearly confirmed as causing PCD were scored.

Statistics

Statistical analysis was performed using Microsoft Excel (www.microsoft.com) and SPSS 22 (www.ibm.com). The mean CBF of each video was assessed using SAVA [21], utilising representative regions of interest (ROI). For each genetic PCD variant, the median CBF, lower/upper quartile and range were determined.

Results

Genetics

Biallelic mutations were identified in 17 genes from 66 PCD subjects of 55 families. 29 subjects exhibited homozygous mutations and 37 individuals exhibited compound heterozygous mutations. Genetic results from 49 individuals have been published previously (see table 1 for references). 19 mutations have not been previously published in the literature or in Ensembl (www.ensembl.org). All mutations resulted in loss-of-function of the respective proteins. All mutations and their functional consequences are shown in table 1.

High-speed video-microscopy analysis

1072 out of 1527 videos from affected individuals (92 out of 130 videos from DCs; 104 out of 125 from HCs) fulfilled the quality control criteria and were therefore analysed. The number of videos available for each gene is presented in table 2. Real-time videos of ciliated nasal epithelial cells are shown in the online supplementary material (videos S1-S19).

Ciliary beat frequency

CBF measurements are summarised in figure 1 and table 2. In the DC group, CBFs ranged 3.95–8.44 Hz with a median frequency of 5.32 Hz; in the HC group, CBFs ranged 4.25–11.63 Hz with a median frequency of 6.36 Hz. CBF in subjects carrying mutations leading to ODA defects (*DNAH5*, *DNAI1*, *DNAI2*, *ARMC4* and *CCDC103*) was severely reduced, with minimal residual ciliary movements in most videos. As an exception, cilia from individual OP-1193 II2 carrying biallelic *CCDC103* mutations were largely completely immotile. In subjects with mutations in *KTU/DNAAF2*, *LRRC50/DNAAF1*, *LRRC6* and *ZMYND10*, which encode assembly factors of ODA/IDA complexes, immotility was invariably observed. By contrast, HVMA yielded heterogeneous findings in individuals carrying *DYX1C1* mutations: in patient F-648 II1, a slightly decreased CBF of 3.45 Hz with maximum values of 7.07 Hz was present, whereas cilia in patient OP-86 II2 were immotile.

In subjects with mutations in *DNAH11*, CBF tended to be increased (median 8.7 Hz (25–75th percentile 6.92–11.31 Hz)). There was a considerable CBF variability (range 1.44–24.86 Hz) with hyperkinetic edges and almost static cilia within the same specimen.

In *CCDC39* and *CCDC40* mutants, SAVA proved unreliable in measuring CBF: median CBF was 2.58 Hz in the *CCDC39* patient and 4.94 Hz for *CCDC40*. In order to further clarify this discrepancy with the obvious visual appearance of an extremely increased frequency, we compared the videos with those from individuals carrying *DNAH11* mutations (increased CBF) and DCs (normal CBF). We found that the CBF was higher in

TABLE 1 Detailed genetic findings in 66 subjects with primary ciliary dyskinesia

Subject	Previously reported	Gene	Mutations	Consequences
F-718 II1	[23]	*DNAH5*	c.[13126-2A>T];[13338+5G>A]	Two splice site mutations
F-668 II1	[23]	*DNAH5*	c.[8029C>T];[8167C>T]	p.Arg2677*+p.Gln2723*
F-661 II1	[24]	*DNAH5*	c.[8910_8911delATinsG];[4361G>A]	Two nonsense mutations p.Ser2970Leufs*7+p.Arg1454Gln Frame shift mutation; missense mutation
F-661 II2	[24]	*DNAH5*	c.[8910_8911delATinsG];[4361G>A]	p.Ser2970Leufs*7+p.Arg1454Gln Frame shift mutation; nonsense mutation
F-658 II2	[24]	*DNAH5*	c.[8440_8447delGAACCAAA]; [8440_8447delGAACCAAA]	p.Glu2814fs*1 Homozygous frame shift mutation
F-373 II4	[24]	*DNAH5*	c.[5563_5564insA];[5563_5564insA]	p.Ile1855Asnfs*5 Homozygous frame shift mutation
F-373 II8	[24]	*DNAH5*	c.[5563_5564insA];[5563_5564insA]	p.Ile1855Asnfs*5 Homozygous frame shift mutation
OP-19 III1	[23]	*DNAH5*	c.[5599_5600insC];[10815delT]	p.Leu1867Profs *35+p.Pro3606Hisfs*22 Two heterozygous frame shift mutations
OP-31 II	[23]	*DNAH5*	c.[4355+1G>A];[5563_5564insA]	p.Ile1855Asnfs*5 Splice site mutation; frame shift mutation
OP-40 II	[23]	*DNAH5*	c.[5147G>T];[13458_13459insT]	p.Arg1716Leu+p.Asn4487fs* Missense mutation; frame shift mutation
OP-51 II1	[23]	*DNAH5*	c.[6791G>A];[13194_13197delCAGA]	p.Ser2264Asn+p.Asp4398Glufs*15 Missense mutation; frame shift mutation
OP-54 II1	[23]	*DNAH5*	c.[2578+1+T>C];[7914_7915insA]	p.Arg2639Thrfs*19 Splice site mutation; frame shift mutation
OP-91 II4	Novel	*DNAH5*	c.[10815delT];**[7897_7902delAGAG]**	p.Pro3606Hisfs*22+p.**Glu2633Alafs*18** Two frame shift mutations
OP-118	Novel	*DNAH5*	c.[8029C>T];**[10813G>A]**	p.Arg2677*+p.**Asp3605Asn** Nonsense mutation; missense mutation
OP-119	Novel	*DNAH5*	c.[5647C>T];**[10384C>T]**	p.Arg1883*+p.**Gln3462*** Two nonsense mutations
OP-226 II4	Novel	*DNAH5*	c.**[3036_3041delAGCG]**;[10815delT]	p.**Val1014Leufs*20**+p.Pro3606Hisfs*22 **Two frame shift mutations**
OP-306	Novel	*DNAH5*	c.[10815delT];[8440_8447delGAACCAAA]	p.Pro3606Hisfs*22+p.Glu2814fs*1 Two frame shift mutations
OP-399 II1	Novel	*DNAH5*	c.**[6343delA];[13193_13198delCAGA]**	p.**Ile2115fs***+**p.Asp4398Glufs*16** **Two frame shift mutations**
OP-486 II1	Novel	*DNAH5*	c.**[11428_11434delACTCA]**;**[10441C>T]**	p.**Asn3810Serfs*21**+**p.Arg358*** **Frame shift mutation; nonsense mutation**
OP-527 II1	Novel	*DNAH5*	c.[10815delT];**[8642C>G]**	p.Pro3606Hisfs*22+**p.Ala2881Gly** Frame shift mutation; **missense mutation**
OP-725 II1	Novel	*DNAH5*	c.**[12265C>T];[2686_2689dup]**	p.**Gln4089***+**p.Glu897Glyfs*4** **Nonsense mutation; frame shift mutation**
OP-815 II2	Novel	*DNAH5*	c.**[4830dup]**;**[4830dup]**	p.**Trp1611Metfs*47** Homozygous frame shift mutation
OP-948 II1	Novel	*DNAH5*	c.**[3037_3040del];[3037_3040del]**	p.**Val1014Leufs20*** **Homozygous frame shift mutation**
OP-1339 II1	Novel	*DNAH5*	c.**[5563dup];[10815_10817delinsCT]**	p.**Ile1855Asnfs*6**+**Pro3606Tyrfs*23** **Two frame shift mutations**
OP-1231 II1	Novel	*DNAH5*	c.**[2291C>A];[2291C>A]**	p.**Ser764*** **Homozygous nonsense mutations**
OP-71 II1	[25]	*DNAI1*	c.[48+2_3insT];[874C>T]	p.Gln292* Splice site mutation; nonsense mutation
OP-121 II1	[25]	*DNAI1*	c.[48+2_3insT];[48+2_3insT]	Homozygous splice site mutation
OP-416 II1	Novel	*DNAI1*	c.[48+2_3insT];[48+2_3insT]	Homozygous splice site mutation
OP-254 II1	[26]	*DNAI2*	c.[787C>T];[787C>T]	p.Arg263* Homozygous nonsense mutation
OP-41 II1	[27]	*DNAH11*	c.[350A>T];[7148T>C]	p.Glu117Val+p. Leu2383Pro Two missense mutations
OP-98 II1	[27]	*DNAH11*	c[.7914G>C];[13333_34insACCA]	p.Trp2604*+p.Ile4445Asnfs*3 Nonsense mutation; frame shift mutation

DOI: 10.1183/09031936.00052014

TABLE 1 Continued

Subject	Previously reported	Gene	Mutations	Consequences
OP-98 II2	[27]	*DNAH11*	c.[7914G>C]; [13333_34insACCA]	p.Trp2604*+p.Ile4445Asnfs*3 Nonsense mutation; frame shift mutation
OP-235 II1	[27]	*DNAH11*	c.[12697C>T];[12980T>C]	p.Gln4233*+p.Leu4327Ser Nonsense mutation; missense mutation
OP-235 II2	[27]	*DNAH11*	c.[12697C>T];[12980T>C]	p.Gln4233*+p.Leu4327Ser Nonsense mutation; missense mutation
OP-263 II1	[8]	*DNAH11*	c.[12384C>G];[13552_13608del]	p.Tyr4128*+p.Ala4518_Ala4523delinsGln Nonsense mutation; deletion/insertion mutation leading to dysfunctional protein
OP-263 II2	[8]	*DNAH11*	c.[12384C>G];[13552_13608del]	p.Tyr4128*+p.Ala4518_Ala4523delinsGln Nonsense mutation; deletion/insertion mutation leading to dysfunctional protein
OP-263 II3	[8]	*DNAH11*	c.[12384C>G];[13552_13608del]	p.Tyr4128*+p.Ala4518_Ala4523delinsGln Nonsense mutation; deletion/insertion mutation leading to dysfunctional protein
OP-263 II4	[8]	*DNAH11*	c.[12384C>G];[13552_13608del]	p.Tyr4128*+p.Ala4518_Ala4523delinsGln Nonsense mutation; deletion/insertion mutation leading to dysfunctional protein
OP-406 II1	[27]	*DNAH11*	c.[84254+5G>T];[4726-1G>A]	Two splice site mutations
OP-406 II2	[27]	*DNAH11*	c.[84254+5G>T];[4726-1G>A]	Two splice site mutations
OP-305 II3	[17]	*HYDIN*	c.[3985G>T];[3985G>T](r.[3985-47_3985-1ins; 3985G>U])	Homozygous splice site mutation
OP-305 II1	[17]	*HYDIN*	c.[3985G>T];[3985G>T](r.[3985-47_3985-1ins; 3985G>U])	Homozygous splice site mutation
OP-305 II2	[17]	*HYDIN*	c.[3985G>T];[3985G>T](r.[3985-47_3985-1ins; 3985G>U])	Homozygous splice site mutation
OP-76 II1	[13]	*CCDC40*	c.[3129delC];[3129delC]	p.Phe1044Serfs*35 Homozygous frame shift mutation
OP-82 II1	[13]	*CCDC40*	c.[248delC];[1810C>T]	p.Ala83Valfs*82+p.Gln604* Frame shift mutation; nonsense mutation
OP-87 II2	[13]	*CCDC40*	c.[248delC]; [778del]	p.Ala83Valfs*82+p.Glu260Argfs*25 Two frame shift mutations
OP-120	[13]	*CCDC40*	c.[248delC];[248delC]	p.Ala83Valfs*82 Homozygous frame shift mutation
OP-240 II2	[13]	*CCDC40*	c.[1315C>T];[1315C>T]	p.Gln439* Homozygous nonsense mutation
F-727 II1	[13]	*CCDC40*	c.[248delC];[248delC]	p.Ala83Valfs*82 Homozygous frame shift mutation
OP-122	[14]	*CCDC39*	c.[1072delA];[1007-1010delAGAA]	p.Thr358Glnfs*3+p.Lys336Argfs*19 Two frame shift mutations
OP-146 II1	[28]	*DNAAF2/KTU*	c.[1214_1215insACGATACCTGCGTGGC]; [1214_1215insACGATACCTGCGTGGC]	p.Gly406Argfs*89 Homozygous frame shift mutation
OP-146 II3	[28]	*DNAAF2/KTU*	c.[1214_1215insACGATACCTGCGTGGC]; [1214_1215insACGATACCTGCGTGGC]	p.Gly406Argfs*89 Homozygous frame shift mutation
OP-234 II1	[28]	*DNAAF2/KTU*	c.[23C>A];[c.23C>A]	p.Ser8* Homozygous nonsense mutation
OP-26 II1	[15]	*CCDC164*	c.[2056A>T];[2056A>T]	p.Lys686* Homozygous nonsense mutation
OP-473 II1	[29]	*DNAAF1/LRRC50*	deletion exon 1+deletion exon 1-12 (compound heterozygous)	Large deletion, no protein
OP-250 II1	Novel	*DNAAF1/LRRC50*	**c.[1349_1350insC];[1349_1350insC]**	**p.Pro451Alafs*5** **Homozygous frame shift mutation**
OP-228 II2	[10]	*LRRC6*	c.[598_599delAA];[598_599delAA]	p.Lys200Glufs*3 Homozygous frame shift mutation
F-637 II3	[6]	*ARMC4*	c.[2712delC];[2712delC]	p.Ile905Leufs*4 Homozygous frame shift mutation
OP-25 II2	[6]	*ARMC4*	c.[2780T>G];[2780T>G]	p.Leu927Trp Homozygous nonsense mutation
OP-38 II1	[6]	*ARMC4*	c.[2675C>A];[2675C>A]	p.Ser892* Homozygous nonsense mutation

TABLE 1 Continued

Subject	Previously reported	Gene	Mutations	Consequences
F-648 II1	[9]	*DYX1C1*	c.[583delA];[583delA]	p.Ile195* Homozygous nonsense mutation
OP-86 II2	[9]	*DYX1C1*	c.[384C>A];[485G>A]	p.Tyr128*+p.Trp162* Two nonsense mutations
OP-55 II1	[10]	*ZMYND10*	Deletion exon 7-12 (homozygous)	Large deletion
OP-225 II2	Novel	*RSPH4A*	c.**[1129delG];[1129delG]**	p.**Glu377Lysfs11*** **Homozygous frame shift mutation**
OP-1193 II2	[7]	*CCDC103*	c.[383_384insG];[383_384insG]	p.Pro129Valfs*24 Homozygous frame shift mutation
OP-1428 II1	Novel	*RSPH1*	c.[275-2A>C];**[433C>T]**	p.**Gln145*** Splice site mutation; **nonsense mutation**

Unpublished mutations are in bold. References are cited for previously reported individuals. Subjects who have not been previously reported are designated as ''novel''. Individuals with identical codes before the Roman letters derive from the same family.

CCDC39 and *CCDC40* (videos S13–S14). Determination of CBF by timing 10 ciliary beat cycles from slow-motion playback of the video files did indeed result in values that were clearly above 15 Hz.

CBF of *CCDC164* mutant cilia was slightly increased with a broad overlap to DCs. In individuals with *HYDIN* mutations, CBF was normal. In individuals with mutations in radial spoke head components, CBF was slightly decreased (*RSPH4A*) or normal (*RSPH1*).

Taken together, CBF values were clearly abnormal in individuals with ODA and ODA/IDA defects. In the other groups, CBF measurement could not distinguish PCD individuals from DCs.

Ciliary beat pattern

A normal beat cycle is characterised by a strong beating stroke followed by a recovery stroke (fig. 2; video S1). Whereas cilia are in a straight position during the beating stroke, the recovery stroke is initiated by bending of the proximal axoneme. Top-view analysis revealed that cilia generally beat within a plane with only small deviations from the longitudinal axis.

Most videos from subjects with ODA defects derived from individuals with *DNAH5* mutations. Typically, *DNAH5* mutant cilia were in a bent position and showed minimal residual movements. Beating of neighbouring cilia was highly uncoordinated (video S2). A similar pattern was observed in other ODA-defect variants (*DNAI1*, *DNAI2*, *ARMC4* and *CCDC103*) (videos S3–S6).

Mutations resulting in combined ODA/IDA defects (*KTU/DNAAF2*, *LRRC50/DNAAF1*, *LRRC6*, *ZMYND10* and *DYX1C1)* resulted in complete ciliary immotility (videos S7–S11). As an exception, individual F-648 II1, who had a homozygous stop mutation in *DYX1C1*, displayed a subtle reduction of the beating amplitude due to an impaired recovery stroke in most videos (video S12), whereas static cilia were present only occasionally.

CBP of subjects with *CCDC39* and *CCDC40* mutations was extremely stiff. A distinction between beating and recovery strokes was not possible (videos S13–S14). *CCDC164* mutant cilia beat with reduced amplitude (video S15) that was much less pronounced than observed in *CCDC39* and *CCDC40*.

Cilia of subjects with *DNAH11* mutations showed a reduced proximal bending (video S16). The degree of stiffness was less pronounced than in *CCDC39/CCDC40* cilia but higher than in *CCDC164* cilia.

HYDIN mutant cilia lacked coordinated beating activity. The bending capacity along the ciliary axoneme was reduced, resulting in decreased beating amplitudes (video S17). Cilia did not generate distinct effective or recovery strokes. In few regions, immotile cilia were also found. A rotatory ciliary movement was observed only occasionally.

In individuals with mutations in radial spoke head components, we found a stiff CBP in a subject with *RSPH4A* mutations (video S18) and in a subject with *RSPH1* mutations (video S19). Circular motion was not seen in *RSPH4A* mutant cilia. In *RSPH1* mutant cilia, circular motion was seen only in a minority of cell clusters.

DOI: 10.1183/09031936.00052014

TABLE 2 Mean ciliary beat frequencies in Hz for genetic primary ciliary dyskinesia variants, disease controls (DCs) and healthy controls (HCs)

Gene	Subjects n	Videos n		Median	Percentile		Min.	Max.
		Recorded	Analysed		25th	75th		
DNAH5	25	351	239	1.12	0	1.26	0	6.53
DNAI1	3	60	28	1.25	1.1	1.49	0	2.2
DNAI2	1	11	9	1.18	1.15	1.24	0	1.39
ARMC4	3	79	52	1.62	1.28	2.26	0	4.37
DNAH11	11	386	260	8.7	6.92	11.31	1.44	24.86
DYX1C1	2	43	42	1.62	0	3.53	0	7.07
DNAAF1/LRRC50	2	53	53	0	0	0	0	0
DNAAF2/KTU	3	66	66	0	0	0	0	0
LRRC6	1	8	8	0	0	0	0	0
ZMYND10	1	9	7	0	0	0	0	0
CCDC103	1	16	5	0	0	0.26	0	1.14
CCDC40	6	74	42	4.94	3.12	5.87	1.04	8.59
CCDC39	1	29	25	2.58	2.41	3.26	1.07	5.85
CCDC164	1	28	19	8.4	5.98	9.91	4.08	12.91
Hydin	3	126	106	4.73	3.01	5.8	1.12	8.69
RSPH4A	1	9	8	1.21	1.16	1.27	1.02	1.44
RSPH1	1	49	11	5.81	5.58	6.53	3.60	8.72
DC	10	130	92	5.32	4.56	6.31	3.95	8.44
HC	10	125	104	6.36	5.57	7.54	4.25	11.63

Discussion

Diagnosing PCD requires a combined approach of complementary methods, all of which have limitations in sensitivity and specificity [1, 3, 4, 30]. Although high-throughput genetic technologies may overcome this in future, many genetic PCD variants remain undiscovered (currently 60–70% of cases can be identified genetically [1]) and this methodology is not yet implemented for routine diagnostics. Because the TEM of

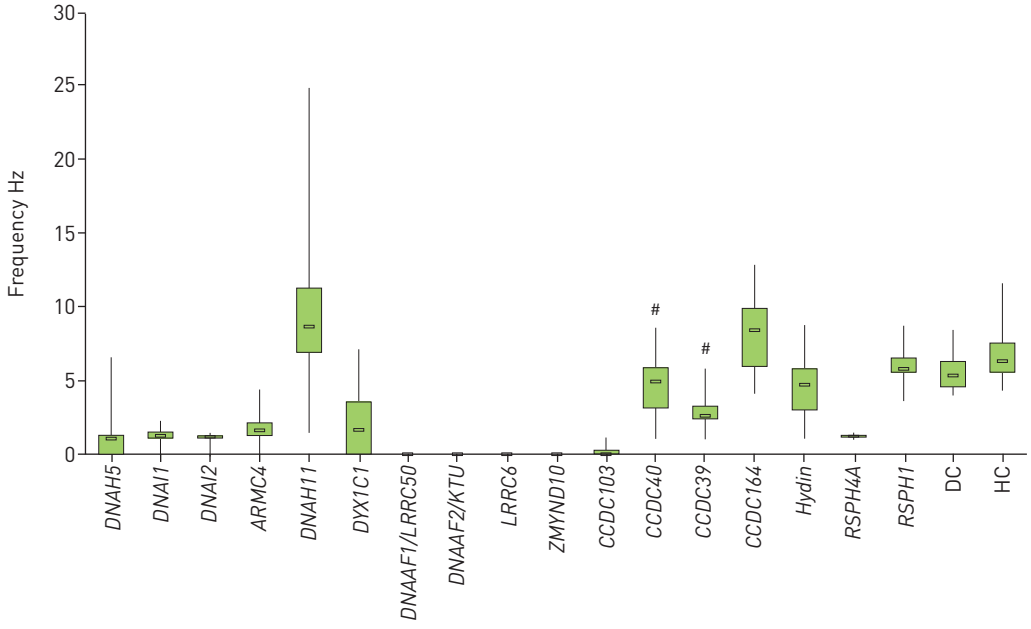

FIGURE 1 Boxplot illustrating ciliary beat frequency (CBF) measured using high-speed video-microscopy analysis in individuals with genetically confirmed primary ciliary dyskinesia sorted according to gene. The bars indicate median CBF values. The boxes respresent 25–75th percentiles. The whiskers indicate maximum and minimum values. DC: disease control. HC: healthy control. #: CBF measurements in *CCDC39* or *CCDC40* mutant cilia yielded implausibly low values using Sisson-Ammens Video Analysis (Ammons Engineering, Mt Morris, MI, USA).

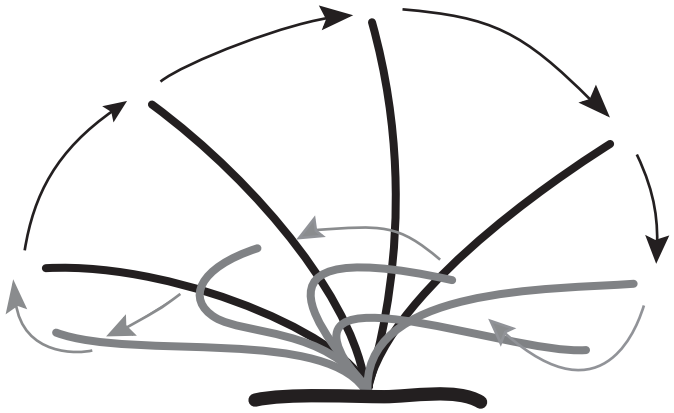

FIGURE 2 Diagram of normal ciliary beat cycle. A normal ciliary beat pattern is characterised by a strong beating stroke (black) followed by a recovery stroke (grey). Whereas the cilia are in a straight position during the beating stroke, the recovery stroke is initiated by a bending of the proximal axoneme.

certain PCD variants is unremarkable [8, 15, 17, 30], HVMA has become the first-line diagnostic test for establishing PCD diagnosis.

HVMA protocols differ among centres in many respects: sampling techniques, microscopes and cameras, temperature during analysis, software, and evaluation criteria. In our study, we used a high-speed video camera at 120–150 fps for capturing video, and SAVA for HVMA analysis. SAVA conveniently allows the determination of CBF and slow-motion video-pattern analysis [21]. We analysed cilia using a total magnification of 400× (resulting from a 40× objective and a 10× ocular lens magnification) at 25°C. Potential disadvantages of this approach include a reduced resolution of cilia as opposed to systems with a higher magnification (1000×). However, using a higher magnification also has potential limitations. Use of 100× objectives (numeric aperture 1.46) results in a markedly reduced depth of focus in the z plane (0.23 µm). Consequently, cilia not recorded strictly from the side may beat outside the range of the focal z plane as shown in video S20, which was captured with a 100× objective. Thus, the limited depth of focus when using a 100× objective bears the risk of misinterpretation of CBPs when the entire ciliary beating cycle is not visualised. This can be avoided by using a 40× objective (numeric aperture 0.56), which has a larger depth of focus of 1.5 µm. In our system, we captured videos at 120 fps, whereas others use cameras with a higher speed of up to 500 fps. Using 120 fps might hinder analyses of very fast ciliary beat variants, a limitation we tried to overcome by analysing CBP at 25°C. This lowers CBF to a point that sufficient images are available for CBP analysis. The ideal temperature for HVMA is also a matter of debate: whereas some centres cool the specimen (because CBP does not change at low temperatures [31] and analyses are facilitated due to the reduced CBF) others perform HVMA at 37°C [32]. However, the temperature in the upper airways increases from about 25°C in the nasal vestibule to 34°C in the nasopharynx [33]. Thus, one might argue that 37°C represents a supra-physiological temperature for nasal-derived cells. We have not systematically compared our protocol with other HVMA systems [31, 34, 35] so it is unclear whether the potential differences are of practical significance. However, our approach enabled us to describe most known subtle PCD variants, such as CP defects [17], isolated nexin link defects [15] and functional ODA defects [8].

SAVA calculates CBF by determination of relative light intensity changes of each pixel within a ROI (as used in this study) or the whole field (whole-field analysis). SAVA only proved inappropriate in samples from individuals with *CCDC39* or *CCDC40* mutations as values were implausibly low. We interpreted this using the extremely stiff CBP. This resulted in only small changes in pixel light intensity that could not be detected accurately using SAVA. Therefore, we recommend a critical visual validation of CBF measurements. Another limitation of HVMA for CBP analysis is the lack of quantitative parameters that describe beat pattern anomalies. Thus, results are dependent on visual interpretation by experienced personnel. Whereas SAVA and other systems are able to quantify CBF, development of quantitative CBP analysis is still at a preliminary stage [36].

In our study, CBF measurement identified PCD variants with severely reduced CBF. However, in these variants, CBP was equally severely altered and discrimination of PCD subjects from unaffected DCs was

DOI: 10.1183/09031936.00052014

readily possible by visual analysis alone. In PCD variants with detectable ciliary motility: 1) mean CBF tended to be increased in *DNAH11* mutant individuals but displayed an overlap with DCs; 2) mean CBF was within the normal range; or 3) CBF measurement was inaccurate (*CCDC39*/*CCDC40*).

In DCs, mean CBF was slightly lower than in HCs, possibly due to the higher degree of secondary dyskinesia. Our values are in line with CBFs measured at 24°C in sinonasal epithelial cells from individuals with chronic sinusitis, where values ranged 3.37–9.13 Hz [37], whereas others have found higher values (7.9 Hz) [34]. These differences might reflect the heterogeneity of HVMA protocols and highlight the need for each centre to carefully determine reference values.

Unlike CBF, CBP analysis nicely correlated with genetic findings and allowed HVMA findings to be classified into different groups, as follows. 1) Combined ODA/IDA defects almost invariably showed complete ciliary immotility. 2) Isolated ODA defects exhibited minimal residual, highly disorganised beating. Completely immotile cilia were seen only occasionally. 3) *CCDC39* and *CCDC40* mutations resulted in an extremely stiff CBP with hardly any amplitude and an increased CBF. 4) *DNAH11* mutations resulted in a hyperkinetic CBP that was less stiff than in *CCDC39* and *CCDC40* mutations. CBF tended to be increased compared to controls. Notably, we also found videos with almost static cilia from *DNAH11* mutants, confirming recent findings in mice [38]. 5) Mutations in *CCDC164* resulted in very subtle HVMA abnormalities. CBP appeared rigid due to reduced amplitude. This phenotype was very mild and could easily be interpreted as normal. 6) Mutations affecting the central pair or radial spoke apparatus have been described as resulting in a circular motion [18, 39] or in a low-amplitude movement [19]. In our PCD subjects, *HYDIN* mutations resulted in rotatory movements only in a minority of ciliary fields. This variant was characterised by a mild reduction of the ciliary bending capacity making it difficult to establish the diagnosis with HVMA alone. The two individuals with *RSPH4A* and *RSPH1* mutations exhibited a stiff CBP with a reduced beating amplitude, a pattern described in *RSPH1* mutations [19]. Circular movements were present only in a minority of cilia in the *RSPH1* subject. Thus, circular ciliary motion is not a compulsory finding in CP or radial spoke defects.

Although typical HVMA findings can be attributed to genetic PCD variants, it should be stressed that phenotypic variations can be found even within one gene, as evidenced in individuals with *DYX1C1* mutations. Similarly, discrepant phenotypes have even been reported in patients with identical genotypes [19], stressing that ciliary beating is not only determined by the molecular defect. Taken together, these findings emphasise that HVMA findings cannot be easily translated to ultrastructural or genetic findings. Thus, additional assays are still necessary to elucidate the underlying mechanisms leading to PCD [6, 9, 15].

Currently, many institutions implement HVMA in order to provide state-of-the-art PCD diagnostics. We hope that our HVMA findings in distinct genetic PCD variants will help disseminate the valuable knowledge necessary for diagnosing PCD. Awareness of the variability of abnormal findings associated with PCD will avoid false-positive as well as false-negative results, and will therefore improve PCD care. Because the interpretation of HVMA findings requires a sufficient sample size of diverse variants, we refer readers to our website pcd.uni-muenster.de, where an extensive, continuously updated collection of HVMA videos of different genetic PCD variants is accessible.

Acknowledgements

We are grateful to the PCD-affected individuals and their families for their participation. We also gratefully acknowledge the German patient support group Kartagener Syndrom und Primaere Ciliaere Dyskinesie e.V. Finally, we thank M. Herting, D. Ernst, K. Vorspohl and S. Helms (all University Children's Hospital Münster, Dept of General Pediatrics, Pediatric Pulmonology Unit, Münster, Germany) for their excellent technical work.

References

1 Knowles MR, Daniels LA, Davis SD, *et al.* Primary ciliary dyskinesia. Recent advances in diagnostics, genetics, and characterization of clinical disease. *Am J Respir Crit Care Med* 2013; 188: 913–922.
2 Kuehni CE, Frischer T, Strippoli M-PF, *et al.* Factors influencing age at diagnosis of primary ciliary dyskinesia in European children. *Eur Respir J* 2010; 36: 1248–1258.
3 Barbato A, Frischer T, Kuehni CE, *et al.* Primary ciliary dyskinesia: a consensus statement on diagnostic and treatment approaches in children. *Eur Respir J* 2009; 34: 1264–1276.
4 Leigh MW, Hazucha MJ, Chawla KK, *et al.* Standardizing nasal nitric oxide measurement as a test for primary ciliary dyskinesia. *Ann Am Thorac Soc* 2013; 10: 574–581.
5 Thomas B, Rutman A, O'Callaghan C. Disrupted ciliated epithelium shows slower ciliary beat frequency and increased dyskinesia. *Eur Respir J* 2009; 34: 401–404.
6 Hjeij R, Lindstrand A, Francis R, *et al.* ARMC4 mutations cause primary ciliary dyskinesia with randomization of left/right body asymmetry. *Am J Hum Genet* 2013; 93: 357–367.
7 Panizzi JR, Becker-Heck A, Castleman VH, *et al.* CCDC103 mutations cause primary ciliary dyskinesia by disrupting assembly of ciliary dynein arms. *Nat Genet* 2012; 44: 714–719.
8 Schwabe GC, Hoffmann ÄK, Loges NT, *et al.* Primary ciliary dyskinesia associated with normal axoneme ultrastructure is caused by DNAH11 mutations. *Hum Mutat* 2008; 29: 289–298.

9 Tarkar A, Loges NT, Slagle CE, *et al.* DYX1C1 is required for axonemal dynein assembly and ciliary motility. *Nat Genet* 2013; 45: 995–1003.
10 Zariwala Ma, Gee HY, Kurkowiak M, *et al.* ZMYND10 is mutated in primary ciliary dyskinesia and interacts with LRRC6. *Am J Hum Genet* 2013; 93: 336–345.
11 Knowles MR, Ostrowski LE, Loges NT, *et al.* Mutations in SPAG1 cause primary ciliary dyskinesia associated with defective outer and inner dynein arms. *Am J Hum Genet* 2013; 93: 711–720.
12 Austin-Tse C, Halbritter J, Zariwala MA, *et al.* Zebrafish ciliopathy screen plus human mutational analysis identifies C21orf59 and CCDC65 defects as causing primary ciliary dyskinesia. *Am J Hum Genet* 2013; 93: 672–686.
13 Becker-Heck A, Zohn IE, Okabe N, *et al.* The coiled-coil domain containing protein CCDC40 is essential for motile cilia function and left-right axis formation. *Nat Genet* 2011; 43: 79–84.
14 Merveille AC, Davis EE, Becker-Heck A, *et al.* CCDC39 is required for assembly of inner dynein arms and the dynein regulatory complex and for normal ciliary motility in humans and dogs. *Nat Genet* 2011; 43: 72–78.
15 Wirschell M, Olbrich H, Werner C, *et al.* The nexin-dynein regulatory complex subunit DRC1 is essential for motile cilia function in algae and humans. *Nat Genet* 2013; 45: 262–268.
16 Horani A, Brody SL, Ferkol TW, *et al.* CCDC65 mutation causes primary ciliary dyskinesia with normal ultrastructure and hyperkinetic cilia. *PLoS One* 2013; 8: e72299.
17 Olbrich H, Schmidts M, Werner C, *et al.* Recessive HYDIN mutations cause primary ciliary dyskinesia without randomization of left-right body asymmetry. *Am J Hum Genet* 2012; 91: 672–684.
18 Castleman VH, Romio L, Chodhari R, *et al.* Mutations in radial spoke head protein genes RSPH9 and RSPH4A cause primary ciliary dyskinesia with central-microtubular-pair abnormalities. *Am J Hum Genet* 2009; 84: 197–209.
19 Kott E, Legendre M, Copin B, *et al.* Loss-of-function mutations in RSPH1 cause primary ciliary dyskinesia with central-complex and radial-spoke defects. *Am J Hum Genet* 2013; 93: 561–570.
20 Ben Khelifa M, Coutton C, Zouari R, *et al.* Mutations in DNAH1, which encodes an inner arm heavy chain dynein, lead to male infertility from multiple morphological abnormalities of the sperm flagella. *Am J Hum Genet* 2014; 94: 95–104.
21 Sisson JH, Stoner JA, Ammons BA, *et al.* All-digital image capture and whole-field analysis of ciliary beat frequency. *J Microsc* 2003; 211: 103–111.
22 O'Callaghan C, Rutman A, Williams GM, *et al.* Inner dynein arm defects causing primary ciliary dyskinesia: repeat testing required. *Eur Respir J* 2011; 38: 603–607.
23 Hornef N, Olbrich H, Horvath J, *et al.* DNAH5 mutations are a common cause of primary ciliary dyskinesia with outer dynein arm defects. *Am J Respir Crit Care Med* 2006; 174: 120–126.
24 Olbrich H, Häffner K, Kispert A, *et al.* Mutations in DNAH5 cause primary ciliary dyskinesia and randomization of left-right asymmetry. *Nat Genet* 2002; 30: 143–144.
25 Zariwala MA, Leigh MW, Ceppa F, *et al.* Mutations of DNAI1 in primary ciliary dyskinesia: evidence of founder effect in a common mutation. *Am J Respir Crit Care Med* 2006; 174: 858–866.
26 Loges NT, Olbrich H, Fenske L, *et al.* DNAI2 mutations cause primary ciliary dyskinesia with defects in the outer dynein arm. *Am J Hum Genet* 2008; 83: 547–558.
27 Knowles MR, Leigh MW, Carson JL, *et al.* Mutations of DNAH11 in patients with primary ciliary dyskinesia with normal ciliary ultrastructure. *Thorax* 2012; 67: 433–441.
28 Omran H, Kobayashi D, Olbrich H, *et al.* Ktu/PF13 is required for cytoplasmic pre-assembly of axonemal dyneins. *Nature* 2008; 456: 611–616.
29 Loges NT, Olbrich H, Becker-Heck A, *et al.* Deletions and point mutations of LRRC50 cause primary ciliary dyskinesia due to dynein arm defects. *Am J Hum Genet* 2009; 85: 883–889.
30 Shoemark A, Dixon M, Corrin B, *et al.* Twenty-year review of quantitative transmission electron microscopy for the diagnosis of primary ciliary dyskinesia. *J Clin Pathol* 2012; 65: 267–271.
31 Smith CM, Hirst RA, Bankart MJ, *et al.* Cooling of cilia allows functional analysis of the beat pattern for diagnostic testing. *Chest* 2011; 140: 186–190.
32 Jackson CL, Goggin PM, Lucas JS. Ciliary beat pattern analysis below 37°C may increase risk of primary ciliary dyskinesia misdiagnosis. *Chest* 2012; 142: 543–544.
33 Keck T, Leiacker R, Riechelmann H, *et al.* Temperature profile in the nasal cavity. *Laryngoscope* 2000; 110: 651–654.
34 Dimova S, Maes F, Brewster ME, *et al.* High-speed digital imaging method for ciliary beat frequency measurement. *J Pharm Pharmacol* 2005; 57: 521–526.
35 Chilvers MA, Rutman A, O'Callaghan C. Functional analysis of cilia and ciliated epithelial ultrastructure in healthy children and young adults. *Thorax* 2003; 58: 333–338.
36 Papon JF, Bassinet L, Cariou-Patron G, *et al.* Quantitative analysis of ciliary beating in primary ciliary dyskinesia: a pilot study. *Orphanet J Rare Dis* 2012; 7: 78.
37 Schipor I, Palmer JN, Cohen AS, *et al.* Quantification of ciliary beat frequency in sinonasal epithelial cells using differential interference contrast microscopy and high-speed digital video imaging. *Am J Rhinol* 2006; 20: 124–127.
38 Lucas JS, Adam EC, Goggin PM, *et al.* Static respiratory cilia associated with mutations in Dnahc11/DNAH11: a mouse model of PCD. *Hum Mutat* 2012; 33: 495–503.
39 Stannard W, Rutman A, Wallis C, *et al.* Central microtubular agenesis causing primary ciliary dyskinesia. *Am J Respir Crit Care Med* 2004; 169: 634–637.

DOI: 10.1183/09031936.00052014